Optomechanics with cavity vacuum fluctuations: Self-alignment and collective rotation mediated by Casimir torque

Denis Ilin,[1,2,3] I. V. Tokatly,[4,5,6] and Ivan Iorsh[1,7]

[1]*School of Mathematical and Physical Sciences, University of Technology Sydney, Ultimo, New South Wales 2007, Australia*
[2]*Sydney Quantum Academy, Sydney, New South Wales 2000, Australia*
[3]*Department of Physics and Technology, ITMO University, St. Petersburg 197101, Russia*
[4]*Nano-Bio Spectroscopy Group and European Theoretical Spectroscopy Facility (ETSF), Departamento de Polímeros y Materiales Avanzados: Física Química y Tecnología, Universidad del País Vasco, Avenida Tolosa 72, E-20018 San Sebastián, Spain*
[5]*IKERBASQUE, Basque Foundation for Science, 48009 Bilbao, Spain*
[6]*Donostia International Physics Center (DIPC), E-20018 Donostia-San Sebastián, Spain*
[7]*Department of Physics, Engineering Physics and Astronomy, Queen's University, Kingston, Ontario K7L 3N6, Canada*

(Received 4 December 2023; revised 3 February 2024; accepted 4 March 2024; published 8 April 2024)

We theoretically consider an ensemble of quantum dimers placed inside an optical cavity. We predict two effects. First, an exchange of angular momentum between the dimers mediated by the emission and reabsorption of the cavity photons leads to the alignment of dimers. Second, the optical angular momentum of the vacuum state of the chiral cavity is transferred to the ensemble of dimers, which leads to the synchronous rotation of the dimers at certain levels of light-matter coupling strength.

DOI: 10.1103/PhysRevA.109.043707

I. INTRODUCTION

The rapidly emerging field of cavity quantum materials [1] explores the routes to tailor the low-energy electronic properties of cavity-embedded low-dimensional materials via engineering of the cavity electromagnetic vacuum fluctuations. The substantial developments in this field were dictated by the tremendous progress in photonic technologies, which allowed routine fabrication of microcavities with large quality factors and extremely small mode volumes, and, therefore, deeply subwavelength field localization. This in turn enabled the regime of the ultrastrong light-matter coupling [2], in which the characteristic energy of light-matter interaction becomes comparable to the cavity photon energy leading to the drastic increase in the role of the vacuum fluctuations. Ultrastrong coupling combined with the collective effects of light-matter coupling was predicted to induce various cavity-mediated phase transitions [3–10] and to modify the chemical reactions [11–14].

The mechanical degrees of freedom play a crucial role in the physics of ultrastrong light-matter coupling for many reasons. First of all, coupling of light to mechanical vibrations in organic molecules can reach an ultrastrong regime even in relatively low quality factor cavities [15–19]. Moreover, recently, the ultrastrong coupling of microwave mechanical vibrations in nanomechanical systems and light was realized in microcavity systems [20,21]. In these setups, a strong nonlinear optomechanical response already emerges at the single-photon pump level. There were several theoretical predictions on the quantum-correlated mechanical motion of atoms in the cavities under weak optical pump [22–25]. Finally, as it is known from the seminal work on the Casimir effect [26], electromagnetic vacuum fluctuations *per se* produce mechanical force. It was recently shown that this force may be utilized for the self-assembly of polarizable nano-objects inside microcavities [27]. Cavity-induced mechanical forces between nano-objects can be regarded as the momentum exchange carried by electromagnetic vacuum fluctuations. As it is known, an electromagnetic field acting on a single scatterer lacking cylindrical symmetry induces both optical force and optical torque. This immediately suggests that the exchange of vacuum electromagnetic fluctuations between asymmetric objects can induce aligning or anti-aligning force. This aligning torque is called Casimir torque, in analogy with the Casimir force induced by vacuum electromagnetic field fluctuations, and has been recently observed experimentally [28]. Moreover, in the case when vacuum electromagnetic fluctuations in a cavity carry nonvanishing angular momentum, it can be transferred to the scatterer and lead to the rotation of the scatterer. Nonvanishing optical angular momentum in the ground state may appear in chiral cavities with broken time-reversal symmetry. If we consider a Fabry-Perot cavity with the mirrors made of ferromagnetic material, the optical modes with opposite circular polarizations will have different frequencies with the energy splitting proportional to magnetization. Ultrastrong light-matter coupling in chiral optical cavities [29] is currently a rapidly developing area of research where multiple novel effects have been proposed, ranging from the cavity-induced anomalous Hall effect [30] to the emergence of peculiar multiphoton correlated states [31].

In this paper, we consider an array of quantum dimers placed inside a chiral optical cavity, as shown in Fig. 1. A dimer could be a biatomic molecule with vanishing static dipole moment or a prolated nano-object [32]. Due to the breaking of time-reversal symmetry, the vacuum state of an electromagnetic field carries nonvanishing angular

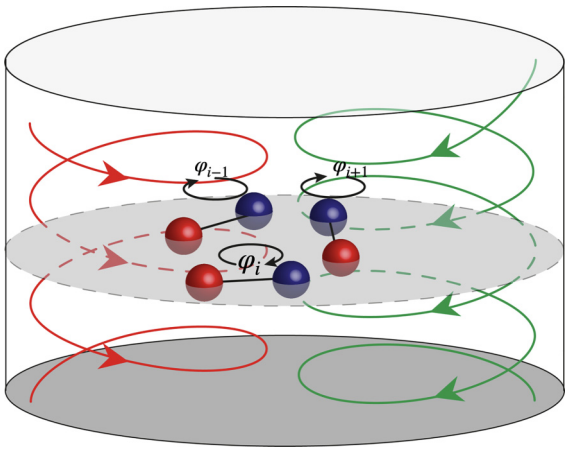

FIG. 1. The geometry of the system. An ensemble of dimers is placed inside a chiral cavity. The orientation of each dimer is defined by the angle φ_i. The dimers may exchange angular momentum via emission and reabsorption of cavity photons. Due to the breaking of time-reversal symmetry, cavity modes of opposite helicity have different energies, which leads to nonvanishing optical angular momentum in the ground state.

momentum, which can be partially transferred to the ensemble of dimers. Moreover, due to the lack of cylindrical symmetry in the dimers, they can exchange angular momentum via emission and reabsorption of cavity photons. In what follows, we provide a quantitative theoretical description of these two effects and show that it leads to the cavity-mediated alignment of dimers and may induces synchronous rotation of the dimers in the cavity.

II. MODEL

We consider an ensemble of N dimers in a cavity. Each dimer is characterized by the resonant frequency Δ and light-matter coupling strength g. We assume that all dimers are located at a single plane parallel to the cavity mirrors. The orientation of each dimer is defined by the angle φ_i. We also allow the dimers to rotate in the plane of the cavity mirrors with moment of inertia J. The full Hamiltonian of the system written in the dipole gauge can be written as

$$\hat{H}_{\rm dip} = \frac{\Delta}{2}\sum_{i=1}^{N}\hat{\sigma}_{z_i} - \sum_{i=1}^{N}\frac{\partial^2_{\varphi_i}}{2J} + \frac{\mathbf{q}^2}{2} + \frac{1}{2}\left(\boldsymbol{\pi} + B[\mathbf{e}_z\times\mathbf{q}] - \frac{g}{2\sqrt{N}}\sum_{i=1}^{N}\hat{\sigma}_{x_i}\mathbf{n}\right)^2, \quad (1)$$

where $\mathbf{q} = (q_x, q_y)$ is the canonical coordinate of the electromagnetic field in the cavity and $\boldsymbol{\pi}$ is the conjugate momentum. The second term in Eq. (1) corresponds to the energy of the mechanical motion of the dimers. $\mathbf{n} = (\cos\varphi_i, \sin\varphi_i)$ is the unit vector defining the orientation of the individual dimer. In the absence of light-matter coupling ($g = 0$), the second line of Eq. (1) corresponds to the gauge-invariant Hamiltonian of the electromagnetic field in the gyrotropic cavity [33] where the parameter B is the time-reversal symmetry-breaking term, which may arise due to, e.g., static magnetization in the cavity mirrors. Light-matter coupling is written in the length gauge within the dipole approximation [34]. The Hamiltonian in Eq. (1) is normalized to the cavity energy ω. We also note that the denominator $\sqrt{N}$ in the term corresponding to light-matter coupling originates from the approximation of constant dimer density. Indeed, coupling strength depends on the mode amplitude, which is inversely proportional to the square root of the mode volume. Therefore, when we keep the density of dimers constant, we need to increase the mode volume proportionally to N, and hence coupling strength scales as $1/\sqrt{N}$. At the same time, one could consider the regime of the constant mode volume (at least for the finite N): in this case, there will be no additional scaling factor $N^{-1/2}$.

For finite N, one could solve the Schrödinger equation with Hamiltonian (1) numerically. Indeed, the system comprises a two-dimensional harmonic oscillator (cavity modes) coupled to N compact continuous variables (angles of the dimers) and to 2^N internal dimer states. Overall, the system comprises 2^N-coupled $(2+N)$-dimensional Schrödinger equations. However, already for small N, one should resort to the approximations such as the Born-Oppenheimer approximation.

As can be seen, the gyrotropy term in the Hamiltonian proportional to B couples cavity modes with linear polarization. It is known that in the presence of the gyrotropy, the nondegenerate eigenmodes of the cavity are those with specific circular polarization. We first apply a unitary transformation (details are presented in Appendix A) in order to diagonalize the cavity part of the Hamiltonian. The diagonalized cavity Hamiltonian then reduces to $\omega_r\hat{r}^\dagger\hat{r} + \omega_l\hat{l}^\dagger\hat{l}$, where r, l correspond to right- and left-circularly polarized modes, $\hat{r}, \hat{l}$ are standard bosonic annihilation operators, and $\omega_{r,l} = \sqrt{B^2+1} \pm B$ (see Appendix A). The operator of the net angular momentum of the cavity modes, which is sometimes referred to as photon spin angular momentum density [35], is given by $\hat{L} = \hat{r}^\dagger\hat{r} - \hat{l}^\dagger\hat{l}$. The Hamiltonian is then written as

$$\hat{H} = \hat{H}_{\rm Mech} + \hat{H}_{\rm Dicke}, \quad (2)$$

where $\hat{H}_{\rm Mech} = (2J)^{-1}\sum_i \hat{p}^2_{\varphi_i}$ corresponds to the mechanic kinetic energy of the dimers and

$$\hat{H}_{\rm Dicke} = \frac{\Delta}{2}\sum_{i=1}^{N}\hat{\sigma}_{z_i} + \omega_r\hat{r}^\dagger\hat{r} + \omega_l\hat{l}^\dagger\hat{l} - \frac{ig/\sqrt{8N}}{\sqrt{\omega_r+\omega_l}}\sum_{i=1}^{N}\hat{\sigma}_{x_i}[\omega_r\hat{r}e^{i\varphi_i} - \omega_l\hat{l}e^{-i\varphi_i}] + \text{H.c.} + \frac{g^2}{8}\left[1 + \frac{1}{N}\sum_{i\neq j}^{N}\hat{\sigma}_{x_i}\hat{\sigma}_{x_j}\cos(\varphi_i - \varphi_j)\right] \quad (3)$$

describes the coupled cavity modes and internal degrees of freedom of the dimers. In order to apply the Born-Oppenheimer (BO) approximation, one omits the $\hat{H}_{\rm Mech}$ at the first step and finds the ground-state energy E_0 of $\hat{H}_{\rm Dicke}$ with orientations of the dimers φ_i treated as parameters, and then adds $E_0(\{\varphi_i\})$ as the potential to $\hat{H}_{\rm Mech}$ to find the mechanical state of the system. It is expected that the BO approximation will be valid for heavy dimers $J \to \infty$.

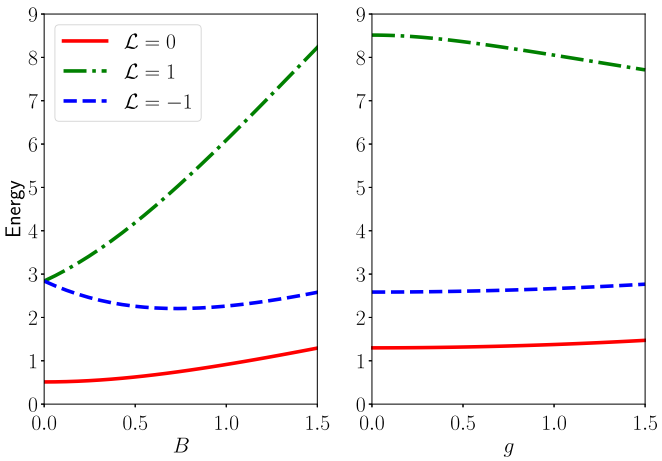

FIG. 2. Dependence of the energy on the total angular momentum on magnetic field B (left panel) and light-matter coupling strength g (right panel). g was set to 0.5 (left panel) and B was set to 1.5 (right panel). The moment of inertia, J, was set to 1 for all cases

We first note that the total angular momentum of the system, $\hat{\mathcal{L}} = \hat{L} + \sum_i p_{\varphi_i}$, is an integral of motion, $[\hat{\mathcal{L}}, \hat{H}] = 0$. For the case of a single qubit, we have solved the Schrödinger equation with the Hamiltonian (1) numerically. Due to the conservation of the total angular momentum, in this case the problem reduces to the two-coupled two-dimensional Schrödinger equations. As can be seen in Fig. 2, the ground state always corresponds to zero total angular momentum. To qualitatively explain the vanishing total angular momentum, one could use the adiabatic argument: indeed, in the absence of light-matter coupling, $g = 0$, the system is equivalent to the Fock-Darwin problem of a parabolic quantum dot in a magnetic field [36]. It is known that the ground state corresponds to the zero total angular momentum. If we adiabatically switch on the coupling, it is expected that the zero angular momentum state will remain the ground state. In what follows, we consider the $\mathcal{L} = 0$ state.

Thus, the total mechanical angular momentum is equal in amplitude and anti-aligned with the optical angular momentum. In Fig. 3(a), the dependence of the optical angular momentum L on the coupling strength g and magnetic field B is plotted for the case of a single dimer. The calculation was performed via numerical solution of the Schrödinger equation with total angular momentum $\mathcal{L} = 0$. It should be noted that for any fixed value of g, the asymptotic of the angular momentum at $B \to \infty$ is $1/B$, and for any fixed value of B asymptotics for $g \to \infty$, it is e^{-g^2}. The large g and B asymptotic analysis is presented in Appendix C.

Since total angular momentum $\mathcal{L}$ is the the integral of motion and it vanishes in the ground state, the uncertainties of the mechanical and optical angular momenta are the same. In Fig. 3(b), we plot the uncertainty of the optical angular momentum as a function of the moment of inertia, J, for the case of a single dimer. The numerical calculation was again performed via the solution of the Schrödinger equation. Small J excitations of the mechanical degrees of freedom cost large energy $(1/J)$ and thus the dimer localizes at the lowest rotational eigenstate, which minimizes the uncertainty

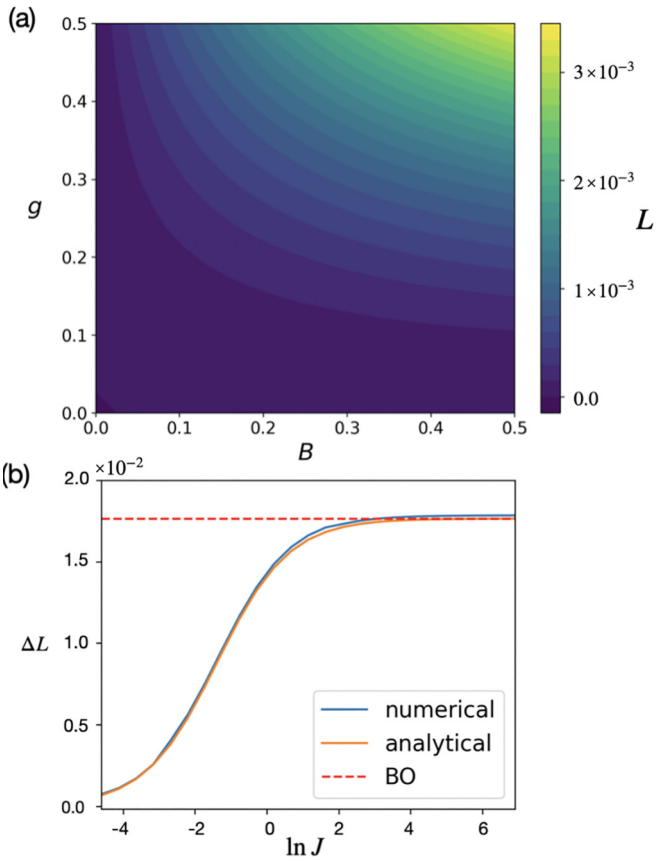

FIG. 3. (a) Dependence of the optical angular momentum L of a single dimer in the ground state on the magnetic field B and coupling strength g. In the calculation, $J = 1 \times 10^6$. (b) Dependence of the uncertainty of the angular momentum on the moment of inertia, J. The dashed horizontal line corresponds to the result obtained within the Born-Oppenheimer approximation (BO). In the calculation, $g = 0.1$, $B = 0.1$. The analytical result was computed with Eq. (5).

of the angular momentum. Since mechanical and optical momenta are rigidly connected, the uncertainty of the optical angular momentum also vanishes. In the opposite limit of heavy dimers, $J \to \infty$, the mechanical kinetic energy can be neglected and the uncertainty is defined by the uncertainty of the photon occupation numbers in the ground state of the Dicke Hamiltonian. As can be seen in Fig. 3(b) for large J, the result of full numerical modeling coincides with the result obtained within the BO approximation. In the case of small light-matter coupling, one may obtain the perturbative result of the optical angular momentum and its uncertainty beyond the BO approximation (see the derivation in Appendix B),

$$L = \frac{g^2\Delta'}{8}\left(\frac{2\omega_r\omega_l + \Delta'(\omega_r+\omega_l)}{(\omega_r+\Delta')^2(\omega_l+\Delta')^2}\right)\frac{\omega_r-\omega_l}{\omega_r+\omega_l}, \tag{4}$$

$$\Delta L = \frac{g}{\sqrt{8}(\omega_r+\omega_l)}\sqrt{\frac{\omega_r^2}{(\Delta'+\omega_r)^2} + \frac{\omega_l^2}{(\Delta'+\omega_l)^2}}, \tag{5}$$

where $\Delta' = \Delta + \frac{1}{2J}$. From Eq. (5), it can be seen that the uncertainty of the angular momentum decreases with the increase of total number of dimers, N. As can be seen in Fig. 3(b), the analytical Eq. (5) approximates the numerical

solution. In what follows, we will resort to the BO approximation since, for the experimentally relevant situations, $J \gg 1$.

We now consider the effective interdimer interaction originating from the coupling to the cavity modes. We focus on the large-N limit describing the gas of dimers. It has been shown in [34] that one may use the $1/N$ expansion for the ground-state energy of the Dicke Hamiltonian. Specifically, the leading correction to the ground-state energy is given by the random phase approximation (RPA),

$$\delta E_0^{RPA} = \int_0^\infty \frac{d\omega}{2\pi} \ln \left\{ \det \left[1 - \frac{g^2}{4N} D_{ph}(i\omega) \sum_{j=1}^{N} \Pi_j(i\omega) \right] \right\}, \tag{6}$$

where D_{ph} is the bare photon propagator and Π_j is the polarization bubble for the jth dimer (expressions for D_{ph} and Π_j are presented in Appendix D).

The integral in Eq. (8) can be taken analytically, yielding

$$\delta E_0^{RPA} = \frac{1}{2} \sum_{l=1}^{4} \omega_{pol,l} - \frac{1}{2}(\omega_r + \omega_l) - \Delta, \tag{7}$$

where $\omega_{pol,l}$ are the energies of the polaritonic modes in the system which are found as the square roots x_l of the zeros of the following fourth-order polynomial presented in Appendix D. In the absence of a magnetic field, the roots can be written compactly, yielding the following expression for the energy correction:

$$\delta E_0^{RPA} = \frac{\Delta + 1}{2} \times \left[\sqrt{1 + \frac{g^2 \Delta (1+Z)}{4(\Delta+1)^2}} + \sqrt{1 + \frac{g^2 \Delta (1-Z)}{4(\Delta+1)^2}} - 2 \right], \tag{8}$$

where $Z = |\frac{1}{N} \sum_{j=1}^{N} e^{2i\varphi_j}|$. It can be seen from Eq. (8) that the dependence of the ground-state energy on the dimer orientation appears only in the term proportional to g^4. The perturbation expansion in g yields the following expression for the orientation-dependent term:

$$\delta E_0(\{\varphi\}) = -\frac{g^4 \Delta^2}{64 N^2} \frac{2\omega_r \omega_l + \Delta(\omega_r + \omega_l)}{(\omega_r + \omega_l)(\omega_r + \Delta)^2 (\omega_l + \Delta)^2} \sum_{i \neq j} \cos^2(\varphi_i - \varphi_j), \tag{9}$$

which, for $B = 0$, coincides with the leading term in the expansion over g of Eq. (8). Within the BO approximation, one needs to solve the Schrödinger equation with the Hamiltonian $\hat{H}_{\text{Mech}} + \delta E_0(\{\varphi\})$ to find the mechanical ground state of the system. For the case of $N = 2$, this problem reduces to solving a one-dimensional Schrödinger equation for the wave function over relative orientation, which is defined by the relative angle $\theta = \varphi_1 - \varphi_2$. The Schrödinger equation is just a Mathieu equation [37] and its ground solutions for different values of g are shown in the insets of Fig. 4. As can be see in Fig. 4, increasing g leads to the localization of the wave-function profiles (shown in insets) and thus the uncertainty of the relative orientation decreases. Uncertainty of the relative angle is directly related to the correlation between the orientations of the dimers: indeed, $\langle \mathbf{n_1 n_2} \rangle = \langle \cos\theta \rangle$.

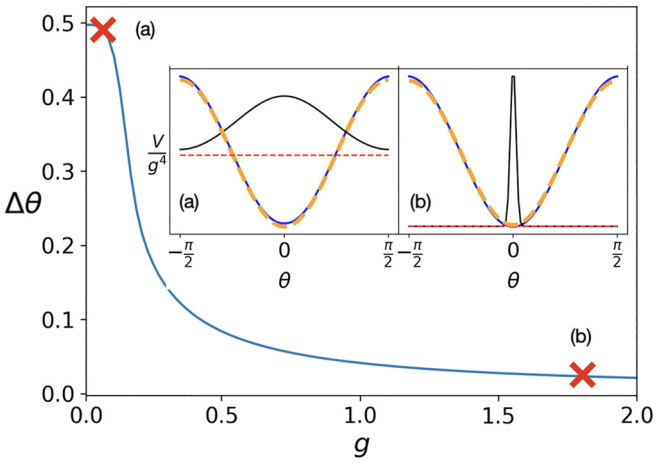

FIG. 4. The dispersion of the difference of two angles, $\theta = \varphi_1 - \varphi_2$, as a function of coupling strength g. Here it is assumed that $\Delta = 1, J = 1 \times 10^7, B = 0.3$. The subplots show mechanical wave functions for the two values of g shown with red crosses on the main plot. On the subplots, solid blue and dashed orange lines show the confining potential obtained via numerical solution of $\hat{H}_{\text{Dicke}}$ within the RPA approximation, respectively, the red dashed line shows the position of the ground-state energy, and the solid black lines depict the profile of the wave function.

We note that the orientation-dependent energy correction in the regime of finite density computed within RPA in Eq. (8) does not scale with N and thus is not an extensive quantity and cannot change the mechanical state of the dimers in the thermodynamic limit, $N \to \infty$. Moreover, even if we consider the case of finite volume, i.e., make substitution $g \to g\sqrt{N}$, the energy correction still scales only as $\sqrt{N}$ and thus is subextensive. This is in accordance with the previously obtained results [34], stating that in the thermodynamic limit, $N \to \infty$, electron photon interaction with a single cavity mode cannot alter the ground state of the electronic system for arbitrary light-matter coupling strength. At the same time, for sufficiently heavy dimers, $J \to \infty$, the cavity-induced Casimir torque can still induce the alignment of the dimers in the cavity. It should be noted that for most of the experimentally realizable systems, $J \gg 1$ ranging from around 100 for the case of light molecules to 1×10^6 for the nano-objects.

It is worthwhile to estimate the feasibility of the discussed effect. A dilute gas of cooled molecules seems to be an appropriate platform. If we approximate the resonant frequency by 1 eV, $\Delta = 1$, $B = 0$ and light-matter coupling strength $g \approx 0.5 \times 10^{-3}$, then the height of the aligning potential for two molecules will be around 1×10^{-13}eV. In the regime of finite mode volume, the height of the potential scales as N, and thus, for $N = 100$, the value is 1×10^{-11}eV, which corresponds to the temperature of approximately 100 nK that is routinely reached in cold-atom experiments. The average distance between the molecules in this case will be of the order of 200 nm and the corresponding collision frequency may be estimated as approximately 10 s^{-1} [38], which is much smaller than the estimated characteristic rotation frequency of

the dimers, which is of the order of 1×10^3 s^{-1}. The cavity-induced alignment effect could be detected as a dependence of the degree of linear polarization of the collective emission from the molecular ensemble as a function of cavity mode volume in a tunable cavity.

III. CONCLUSION

To conclude, we have shown that the collective light-matter coupling of an ensemble of dimers in a two-mode cavity leads to the emergence of the Casimir torque forcing to align the dimers along a single direction. Moreover, in the case of a chiral cavity, when there exists an energy splitting between the two circularly polarized modes, the light-matter interaction induces a torque that leads to the coherent rotation of the ensemble. In the future, it is worthwhile to consider the torque emerging between two dissimilar group of dimers, where, as has been recently shown, strong correlations beyond the RPA approximation may arise [39]. It is also worth noting that the effective Hamiltonian for the mechanical motion is that of a fully connected quantum rotor model, which has recently drawn considerable attention in the context of quantum criticality [40]. Therefore, we believe that the proposed effect could find its applications in quantum simulations of the correlated phases with cavity-embedded cold atoms.

ACKNOWLEDGMENTS

We are grateful to A. Kudlis for useful discussions. I.V.T. acknowledges support from Grupos Consolidados UPV/EHU del Gobierno Vasco (Grant No. IT1453-22) and from Grant No. PID2020-112811GB-I00 funded by MCIN/AEI/10.13039/501100011033. Also, we acknowledge support from the "Basis" Foundation (Grant No. 21-1-2-61-4).

APPENDIX A: DIAGONALIZATION OF THE EMPTY CAVITY HAMILTONIAN. BOGOLIUBOV TRANSFORMATION

In the main text of this paper, it is noticed that in order to fully diagonalize a cavity Hamiltonian, we need to implement the Bogoliubov transformation, taking into account all orders of field B. So the exact transformation is

$$U_B = \begin{pmatrix} u_1 & u_1 & -u_2 & -u_2 \\ iu_1 & -iu_1 & iu_2 & -iu_2 \\ -u_2 & -u_2 & u_1 & u_1 \\ -iu_2 & iu_2 & -iu_1 & iu_1 \end{pmatrix}, \tag{A1}$$

where

$$u_1 = \frac{2+\omega_r+\omega_l}{4\sqrt{\omega_r+\omega_l}},\ u_2 = \frac{(\omega_r-\omega_l)^2}{4\sqrt{\omega_r+\omega_l}(2+\omega_r+\omega_l)}. \tag{A2}$$

Here we suppose $\omega_{r,l} = \sqrt{1+B^2} \pm B$. Also note that $\omega_{r,l}$ are values that normalized to the frequency of incoming photons, so these values are dimensionless.

APPENDIX B: PERTURBATION THEORY FOR THE CASE OF WEAK LIGHT-MATTER COUPLING

In this Appendix, we consider a weak light-matter coupling regime, where one can use the perturbation expansion in coupling constant g. The weak interaction is described by the relationship $g \ll \Delta$. In this case, we can consider parts that are proportional to the coupling strength g as some perturbation potentials and exploit the results from the perturbation theory. Note that this problem is solved without taking into account the Born-Oppenheimer approximation. The Hamiltonian reads

$$\begin{aligned} \hat{H} &= \hat{H}_0 + g\hat{V}_1 + g^2\hat{V}_2, \\ \hat{H}_0 &= \sum_{i=1}^{N} \frac{\hat{p}_{\varphi_i}^2}{2J} + \frac{\Delta}{2}\left(\sum_{i=1}^{N} \hat{\sigma}_{z_i}\right) + \omega_r \hat{r}^\dagger \hat{r} + \omega_l \hat{l}^\dagger \hat{l}, \end{aligned} \tag{B1}$$

where

$$\hat{V}_1 = -\frac{i}{\sqrt{8N(\omega_r+\omega_l)}} \sum_{i=1}^{N} \hat{\sigma}_{x_i}(\omega_r \hat{r} e^{i\hat{\varphi}_i} - \omega_l \hat{l} e^{-i\hat{\varphi}_i}) + \text{H.c.}, \quad \hat{V}_2 = \frac{1}{8}\left[1 + \frac{1}{N}\sum_{i\neq j}^{N} \cos(\hat{\varphi}_i - \hat{\varphi}_j)\hat{\sigma}_{x_i}\hat{\sigma}_{x_j}\right]. \tag{B2}$$

The unperturbed part can be easily diagonalized as

$$E_{n,m,M,\mathbf{k}} = \sum_{i=1}^{N} \frac{k_i^2}{2J} + \Delta M + \omega_r n + \omega_l m, \quad \Psi_{n,m,M,\mathbf{k}} = \left\{\prod_{i=1}^{N} e^{ik_i\varphi_i}\right\} |n\rangle_r |m\rangle_l |M\rangle. \tag{B3}$$

Here we denote $|n\rangle_{r(l)}$ as the Fock state of the $r(l)$ mode, M is the total spin projection on the z axis and $|M\rangle$ is the eigenstate of the operator $\sum_i \hat{\sigma}_{z_i}$, $k_i \in \mathbb{Z}$ is the eigenvalue for operator $\hat{p}_i$, and $\mathbf{k} = (k_1, \ldots, k_N)^T$. The matrix elements of the perturbation

operators read

$$\langle n', m', \mathbf{k}'|\hat{V}_1|n, m, \mathbf{k}\rangle = \frac{i}{\sqrt{8N(\omega_r+\omega_l)}}(\omega_l\sqrt{m}\delta_{n',n}\delta_{m',m-1} - \omega_r\sqrt{n+1}\delta_{n',n+1}\delta_{m',m})\sum_{i=1}^{N}\hat{\sigma}_{x_i}e^{-i\varphi_i}\delta_{k_i',k_i+1}$$
$$+ \frac{i}{\sqrt{8N(\omega_r+\omega_l)}}(\omega_l\sqrt{m+1}\delta_{m',m+1}\delta_{n',n} - \omega_r\sqrt{n}\delta_{n',n-1}\delta_{m',m})\sum_{i=1}^{N}\hat{\sigma}_{x_i}e^{i\varphi_i}\delta_{k_i',k_i-1},$$
$$\langle n', m', \mathbf{k}'|\hat{V}_2|n, m, \mathbf{k}\rangle = \frac{1}{8}\left[1+\frac{1}{N}\sum_{i\neq j}^{N}\cos(\varphi_i-\varphi_j)\hat{\sigma}_{x_i}\hat{\sigma}_{x_j}\right]\delta_{n,n'}\delta_{m,m'}\delta_{\mathbf{k}',\mathbf{k}}, \tag{B4}$$

where $\delta_{m',m+1}$ is the Kronecker symbol. For the ground state of the perturbed system, we obtain the expansion

$$E_0 = E_0^0 + g^2E_2^2 + g^3E_0^3 + g^4E_0^4 + \cdots, \quad E_0^0 = -\frac{\Delta}{2}N,$$
$$\Psi_0 = \Psi_0^{(0)} + g\Psi_0^{(1)} + g^2\Psi_0^{(2)} + g^3\Psi_0^{(3)} + \cdots, \quad \Psi_0^{(0)} = \left\{\prod_{i=1}^{N}e^{ik_i\varphi_i}\delta_{k_i}\right\}|0\rangle_r|0\rangle_l\Big|-\frac{N}{2}\Big\rangle. \tag{B5}$$

For the second correction, we have

$$E_0^2 = \langle 0|\hat{V}_2|0\rangle + \sum_{s_1\neq 0}\frac{\left|\langle s_1|\hat{V}_1|0\rangle\right|^2}{E_0^0-E_{s_1}^0} = \frac{\Delta'}{8}\frac{2\omega_r\omega_l+\Delta'(\omega_l+\omega_l)}{(\omega_r+\omega_l)(\omega_r+\Delta')(\omega_l+\Delta')}, \tag{B6}$$

where a state $s_1 = \{n, m, M, \mathbf{k}\}$ is parameterized by the eigenvalues set and $\Delta' = \Delta + \frac{1}{2J}$. For the next correction, we obtain

$$E_0^3 = \sum_{s_1\neq 0}\frac{\langle 0|\hat{V}_2|s_1\rangle\langle s_1|\hat{V}_1|0\rangle + \langle 0|\hat{V}_1|s_1\rangle\langle s_1|\hat{V}_2|0\rangle}{E_0^0-E_{s_1}^0} + \sum_{s_1,s_2\neq 0}\frac{\langle 0|\hat{V}_1|s_1\rangle\langle s_1|\hat{V}_1|s_2\rangle\langle s_2|\hat{V}_1|0\rangle}{\left(E_0^0-E_{s_1}^0\right)\left(E_0^0-E_{s_2}^0\right)} = 0. \tag{B7}$$

The most interesting part appears in the fourth part, i.e., the dependence on phases,

$$E_0^4 = \sum_{s_1,s_2,s_3\neq 0}\frac{\langle 0|\hat{V}_1|s_1\rangle\langle s_1|\hat{V}_1|s_2\rangle\langle s_2|\hat{V}_1|s_3\rangle\langle s_3|\hat{V}_1|0\rangle}{\left(E_n^0-E_{s_1}^0\right)\left(E_n^0-E_{s_2}^0\right)\left(E_n^0-E_{s_3}^0\right)} - \langle 0|\hat{V}_2|0\rangle\sum_{s_1\neq 0}\frac{|\langle s_1|\hat{V}_1|0\rangle|^2}{\left(E_0^0-E_{s_1}^0\right)^2} - \sum_{s_1\neq 0}\frac{|\langle s_1|\hat{V}_1|0\rangle|^2}{\left(E_0^0-E_{s_1}^0\right)^2}\sum_{s_1\neq 0}\frac{|\langle s_1|\hat{V}_1|0\rangle|^2}{E_0^0-E_{s_1}^0}$$
$$+ \sum_{s_1\neq 0}\frac{\langle 0|\hat{V}_2|s_1\rangle\langle s_1|\hat{V}_1|s_2\rangle\langle s_2|\hat{V}_1|0\rangle + \langle 0|\hat{V}_1|s_1\rangle\langle s_1|\hat{V}_2|s_2\rangle\langle s_2|\hat{V}_1|0\rangle + \langle 0|\hat{V}_1|s_1\rangle\langle s_1|\hat{V}_1|s_2\rangle\langle s_2|\hat{V}_2|0\rangle}{\left(E_n^0-E_{s_1}^0\right)\left(E_n^0-E_{s_2}^0\right)} + \sum_{s_1\neq 0}\frac{|\langle s_1|\hat{V}_2|0\rangle|^2}{E_0^0-E_{s_1}^0}. \tag{B8}$$

From here, we obtain a part without phases (A) and with phases,

$$E_0^4 = A - \frac{\Delta'^2}{64N^2}\frac{2\omega_r\omega_l+\Delta'(\omega_r+\omega_l)}{(\omega_r+\omega_l)(\omega_r+\Delta')^2(\omega_l+\Delta')^2}\sum_{i\neq j}\cos^2(\varphi_i-\varphi_j). \tag{B9}$$

As we can see, the part with phases is nonpositive, which means that the minimum is when all phases are equal, i.e., all qubits tends to rotate in-phase. Speaking of the angular momentum of the system, we can find it in the second order in expansion on g, i.e.,

$$L \approx \left\langle\Psi_0^{(0)} + g\Psi_0^{(1)}|\hat{L}|\Psi_0^{(0)} + g\Psi_0^{(1)}\right\rangle = \frac{g^2\Delta'}{8}\left(\frac{2\omega_r\omega_l+\Delta'(\omega_r+\omega_l)}{(\omega_r+\Delta')^2(\omega_l+\Delta')^2}\right)\frac{\omega_r-\omega_l}{\omega_r+\omega_l}, \tag{B10}$$

and dispersion,

$$\Delta L \approx \frac{g}{\sqrt{8(\omega_r+\omega_l)}}\sqrt{\frac{\omega_r^2}{(\Delta'+\omega_r)^2}+\frac{\omega_l^2}{(\Delta'+\omega_l)^2}}. \tag{B11}$$

As can be seen, it is proportional to the difference between two energies, $\omega_r - \omega_l = 2B$, i.e., the existence of the angular momentum is the result of the presence of nonzero B in the system. On the other hand, if there is tremendous field B in the system, then the angular momentum decreases as $L \approx \frac{g^2}{16B}$. As a result, the maximum angular momentum is reached somewhere in the middle. As can be seen from Fig. 5, even for not very small coupling strength $g = 0.5$, the angular momentum is still very low, i.e., less than 5×10^{-3}.

APPENDIX C: PERTURBATION THEORY FOR THE CASE OF STRONG LIGHT-MATTER COUPLING

In this Appendix, we consider the strong interaction $\Delta < g$ in the presence of the weak field $B \ll g$. Such regime can be realized in practice for relatively small detuning Δ. In this situation, it is possible to consider the part that is proportional

to the total z-spin projection as a perturbation. For simplicity, we demonstrate the derivation for the $N = 1$ qubit in detail. The Hamiltonian after transformation will be

$$\hat{H}_{N=1} = \frac{(\hat{p}_\varphi - \hat{L})^2}{2J} + \frac{\Delta}{2}\hat{\sigma}_z + \omega_r \hat{r}^\dagger \hat{r} + \omega_l \hat{l}^\dagger \hat{l} - \frac{ig}{\sqrt{8(\omega_r + \omega_l)}}\hat{\sigma}_x[\omega_r(\hat{r} - \hat{r}^\dagger) - \omega_l(\hat{l} - \hat{l}^\dagger)] + \frac{g^2}{8}. \tag{C1}$$

Then we implement the Born-Oppenheimer approximation, so we omit the part that corresponds to the mechanical motion and we also make a rotation such that $\hat{\sigma}_x \to \hat{\sigma}_z$, $\hat{\sigma}_z \to -\hat{\sigma}_x$. After that, we obtain

$$\hat{H}^{N=1}_{\text{Dicke}} = \hat{H}_0 + \hat{V} = \omega_r \hat{r}^\dagger \hat{r} + \omega_l \hat{l}^\dagger \hat{l} - \frac{ig}{\sqrt{8(\omega_r + \omega_l)}}\hat{\sigma}_z[\omega_r(\hat{r} - \hat{r}^\dagger) - \omega_l(\hat{l} - \hat{l}^\dagger)] + \frac{g^2}{8} - \frac{\Delta}{2}\hat{\sigma}_x, \tag{C2}$$

where $\hat{V} = -\frac{\Delta}{2}\hat{\sigma}_z$. The unperturbed part can be easily diagonalized as

$$E_{n,m} = \omega_r n + \omega_l m,$$
$$\Psi_{n,m} = \{|\uparrow\rangle|n\rangle_{-iq}|m\rangle_{iq},\ |\downarrow\rangle|n\rangle_{iq}|m\rangle_{-iq}\},$$
$$q = \frac{g}{\sqrt{8(\omega_r + \omega_l)}}, \tag{C3}$$

where $|n\rangle_r$ denotes the Fock state of the displaced oscillator on r. As we can see, in an unperturbed system, every level is twice degenerate. The existence of the perturbation removes the degeneracy and then we obtain

$$E_{n,m,\pm} = \omega_r n + \omega_l m \mp \frac{\Delta}{2} e^{-4q^2} L_n(4q^2) L_m(4q^2),$$
$$\Psi^{(0)}_{n,m,\pm} = \frac{1}{\sqrt{2}}(|\uparrow\rangle|n\rangle_{-iq}|m\rangle_{iq} \pm |\downarrow\rangle|n\rangle_{iq}|m\rangle_{-iq}), \tag{C4}$$

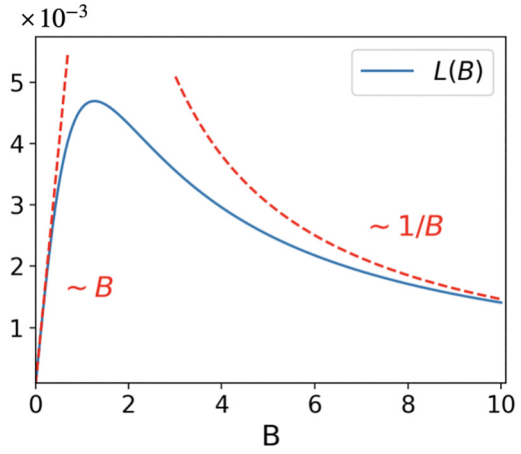

FIG. 5. The angular momentum as a function of the field B. We supposed here that the incoming photon is resonant with the ground-state to excited-state transition of qubits, i.e., $\Delta = 1$, and fixed the coupling strength $g = 0.5$.

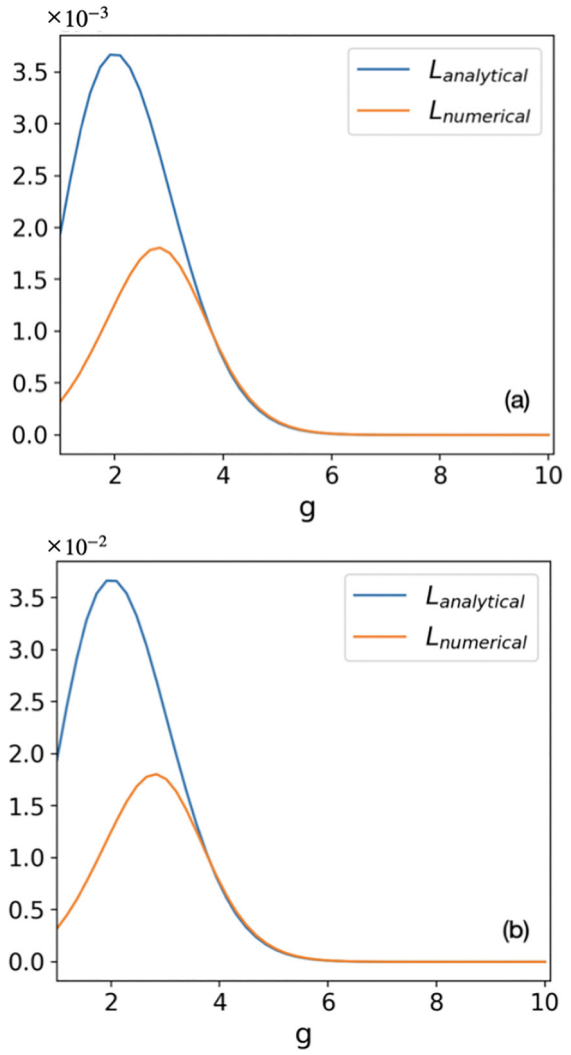

FIG. 6. Comparison of the analytically calculated angular momentum for the $N = 1$ qubit as a function of coupling strength g and numerically calculated for the cases (a) $B = 0.01$ and (b) $B = 0.1$, both for $\Delta = 1$. As can be seen, the angular momentum is proportional to B, even for big g. The biggest difference between the analytical and numerical results occurs in the vicinity of the maximal angular momentum.

where $L_n(x)$ is the Lauguere polynomial. So the ground energy is

$$E^0_0 = -\frac{\Delta}{2} e^{-4q^2},$$
$$\Psi^0_0 = \frac{1}{\sqrt{2}}(|\uparrow\rangle|0\rangle_{-iq}|0\rangle_{iq} + |\downarrow\rangle|0\rangle_{iq}|0\rangle_{-iq}). \tag{C5}$$

Before we go further, it is wise to make a comment. Use of the perturbation theory in this way is only valid when splitting the energy levels by perturbation is small compared to the main levels, i.e., $\omega_l \gg \Delta e^{-4q^2}$. It can be deduced that if $q \gg 1$, then $g \gg \sqrt{\omega_r + \omega_l}$ or simply $g \gg B$.

For our purposes, it is sufficient to consider only the first order on Δe^{-4q^2} in the wave function to find the nonzero value for the angular momentum. So we introduce the expansion for

the ground state,

$$\Psi_0 = \Psi_0^{(0)} + \Delta e^{-4q^2}\Psi_0^{(1)} + \cdots,$$
$$\Psi_0^{(1)} = \frac{1}{4}\sum_{n\neq m}\frac{(2q)^{n+m}}{\sqrt{n!m!}(\omega_r n + \omega_l m)} \times \left\{[1+(-1)^{n+m}]\Psi^{(0)}_{n,m,+} - [1-(-1)^{n+m}]\Psi^{(0)}_{n,m,-}\right\}. \tag{C6}$$

From here, we can find the angular momentum, up to the first order of Δe^{-4q^2},

$$L_1 = \left\langle \Psi_0^{(0)} + g\Psi_0^{(1)}|\hat{L}|\Psi_0^{(0)} + g\Psi_0^{(1)}\right\rangle \approx 4B\Delta q^2 e^{-4q^2}, \tag{C7}$$

$$\Delta L_1 \approx \sqrt{2(\omega_r+\omega_l)\Delta}\, q e^{-2q^2}. \tag{C8}$$

Again we see that the occurrence L is a consequence of the existence of the field B in the system. Also, in the case of a tremendous value of the coupling strength g and some fixed field B, the angular momentum will decrease rapidly. This fact is also a hint that the maximal possible value is somewhere in the middle; see Fig. 6.

Such derivation can be realized for any number of qubits in the system. Here we also represent the analytically counted angular momentum for the system with $N = 2$ qubits,

$$L_2 \approx 4B\Delta q^2 e^{-2q^2}. \tag{C9}$$

Furthermore, it is proved numerically that in systems with N qubits, we will have $L_N \approx 4B\Delta q^2 e^{-\frac{4}{N}q^2}$.

We now consider an intermediate regime, when the splitting of energy levels due to the spin $\hat{V} = -\Delta\hat{S}_x$ and energy levels of the l mode are very close to each other such that some energy levels become degenerated. For example, in the system with $N = 1$ qubit, it means $\omega_l \approx \Delta e^{-4q^2}$; see Fig. 7. We call this regime intermediate. Mathematically, it means that we cannot use the perturbation theory as we did. Instead, we need to honestly diagonalize the matrix in the vicinity of level degeneracy.

Now we are going to provide a full derivation for the system with a $N = 1$ qubit, taking into account an explicit diagonalization of only the zero and the first excitation of the d mode. So, in order to find the ground state, we should find the minimal eigenvalue of the matrix,

$$H = \begin{pmatrix} 0 & -\frac{\Delta}{2}e^{-4q^2} & 0 & i\Delta q e^{-4q^2} \\ -\frac{\Delta}{2}e^{-4q^2} & 0 & -i\Delta q e^{-4q^2} & 0 \\ 0 & -i\Delta q e^{-4q^2} & \omega_l & -\frac{\Delta}{2}e^{-4q^2}L_1(4q^2) \\ i\Delta q e^{-4q^2} & 0 & -\frac{\Delta}{2}e^{-4q^2}L_1(4q^2) & \omega_l \end{pmatrix}. \tag{C10}$$

Previously we omitted the excited levels of the l mode. Now we consider the case when the energy of the first excited state of the l mode is small enough such that

$$\omega_l + \frac{\Delta}{2}e^{-4q^2}L_1(4q^2) \approx \frac{\Delta}{2}e^{-4q^2} \;\leftrightarrow\; \omega_l = 2q^2\Delta e^{-4q^2}. \tag{C11}$$

This relation is in a good match with the results from the straightforward numerical modulation of the system; see Fig. 8(a). After that, we can find the ground energy as $E_0 = -\frac{\Delta}{2}e^{-4q^2}\sqrt{1+4q^2}$ and the state as

$$\Psi_0 = \frac{q}{\sqrt{1+4q^2+\sqrt{1+4q^2}}} \times \left\{-|\uparrow\rangle|0\rangle_{-iq}|1\rangle_{iq} + |\downarrow\rangle|0\rangle_{iq}|1\rangle_{-iq} + \frac{1+\sqrt{1+4q^2}}{2q}|\uparrow\rangle|0\rangle_{-iq}|0\rangle_{iq} + \frac{1+\sqrt{1+4q^2}}{2q}|\downarrow\rangle|0\rangle_{iq}|0\rangle_{-iq}\right\}. \tag{C12}$$

Using this state, we can derive the angular momentum,

$$L_1 \approx \langle\Psi_0|\hat{L}|\Psi_0\rangle = \frac{2q^2}{1+\sqrt{1+4q^2}}. \tag{C13}$$

As it can be seen, this estimation already gives huge values such as $L_1 > 0.1$. Please note that this formula cannot be used for very small fields B because the angular momentum does not vanish. Nevertheless, the numerical model predicts that the real values of L are larger than this estimation and so it is not sufficient to achieve the precise result taking into account only the interaction of the zero and first excitations. However, this procedure can be spread to the larger number of excitations. Indeed, let the ground state be described by mixing first $n-1$ excitations and the ground state,

$$\Psi_0 \approx \sum_{j=0}^{n-1} C_j^{\uparrow}|\uparrow\rangle|0\rangle_{-iq}|j\rangle_{iq} + C_j^{\downarrow}|\downarrow\rangle|0\rangle_{iq}|j\rangle_{-iq}, \tag{C14}$$

where $C_i^{\uparrow;\downarrow}$ are complex normalized coefficients, so $|\Psi_0|^2 = 1$. After some algebra, we can obtain

$$L_1 \approx \langle\Psi_0|\hat{L}|\Psi_0\rangle = -\sum_{j=1}^{n-1}\{j[|C_j^{\uparrow}|^2 + |C_j^{\downarrow}|^2] + 2q\sqrt{j}[C_j^{\uparrow *}C_{j+1}^{\uparrow} - C_j^{\downarrow *}C_{j-1}^{\downarrow}]\}. \tag{C15}$$

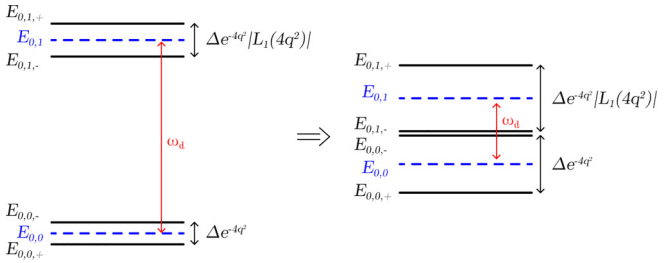

FIG. 7. The left part (II) region, i.e., the splitting levels due to the Δ part are small compared to the excitations of the l mode. The right part is the resonance regime, i.e., they are of the same order.

Then, using this formula, we can calculate corrections to the angular momentum; see Fig. 8(b). As can be seen, it is sufficient to predict the real value of the angular momentum considering the mixing of the first nine excitations and the ground state.

Despite the fact that it is possible to find an intermediate solution for any large (g, B) for the fixed Δ, there are several restrictions on the occurrence of the intermediate regime in the systems with small g, B. Indeed, the two main relationships should be preserved in order to observe the intermediate solution, i.e., the condition of appliance of the perturbation theory and degeneracy of level splitting due to the spin perturbation potential. Altogether, it leads to the more interpreted condition, i.e., $q \geqslant 1/2$. So it can be rewritten as

$$\frac{g^4}{16} \geqslant 1 + B^2,$$
$$\Delta \geqslant 2e\omega_l. \tag{C16}$$

The first inequality means that the intermediate solution takes place for any field B, but only for coupling strengths that are greater than 2, i.e., $g \geqslant 2$. Finding such state in real systems is the main problem because of the practical difficulties to achieve such strength in real systems. The second inequality means that it is not possible for all small frequencies to observe such regime. This happens mostly because of the restriction on g.

For the system with $N = 2$ qubits, it is only possible to analytically write the intermediate condition [see Fig. 8(a)],

$$\omega_l \approx \Delta e^{-2q^2}. \tag{C17}$$

Nevertheless, we can say that for the system with N qubits, when all of them are in phase, i.e., $\varphi_i = \varphi_j$ for any i, j and fixed field B, the angular moments are connected by the relationship $L_N = \sqrt{N} L_1$. This relation is proven numerically for several systems. Also it implies an interesting thing. We can achieve the target angular momentum by decreasing field B and increasing coupling strength g and the number of qubits, N, in the system. This effect might be very useful in future applications.

The intermediate state is also remarkable due to the fact that the angular momentum attains its maximal value in this state with two fixed parameters, i.e., Δ, B or Δ, g. In Fig. 9, we numerically calculated the angular momentum for different B, g with fixed $\Delta = 1$ for $N = 1$ [Fig. 9(a)] and $N = 2$ [Fig. 9(b)]. As can be seen, the maximal values on the verticals or horizontals are achieved in the intermediate state.

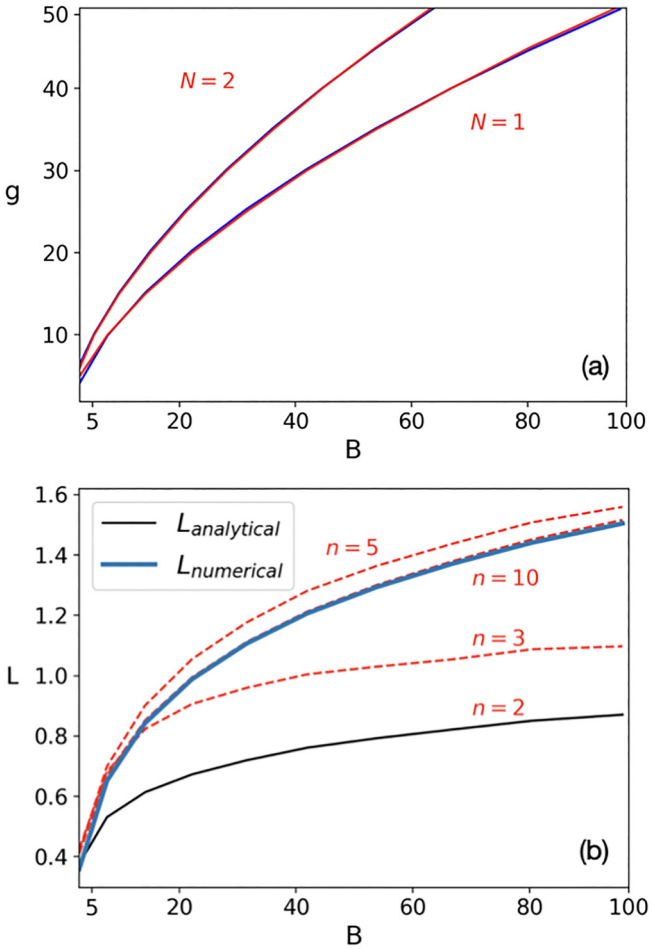

FIG. 8. (a) The dependence between field B and coupling strength g assuming the incoming photons are resonant with the qubits, i.e., $\Delta = 1$. Red lines correspond to the analytical resonance relationships for $N = 1$ and $N = 2$, respectively, and blue lines correspond to the numerical solution. (b) The maximal possible angular momentum for the resonant photons, i.e., $\Delta = 1$, as a dependence on field B for the $N = 1$ system. The blue line corresponds to numerical solution, the black line is the simplest analytical model (C13), and the red lines are the solution of (C15) taking into account the interaction between the first $n - 1$ excitations.

APPENDIX D: GROUND-STATE ENERGY CORRECTION WITHIN THE RANDOM PHASE APPROXIMATION

In this Appendix, we derive the ground-state energy correction due to the light-matter coupling in the limit of large number of dimers, $N \to \infty$. As has been shown in [34], this energy correction is governed by the random phase approximation. Specifically,

$$\delta E_0^{RPA} = \int_0^\infty \frac{d\omega}{2\pi} \ln \left\{ \det \left[1 - \frac{g^2}{4N} D_{ph}(i\omega) \sum_{j=1}^{N} \Pi_j(i\omega) \right] \right\}, \tag{D1}$$

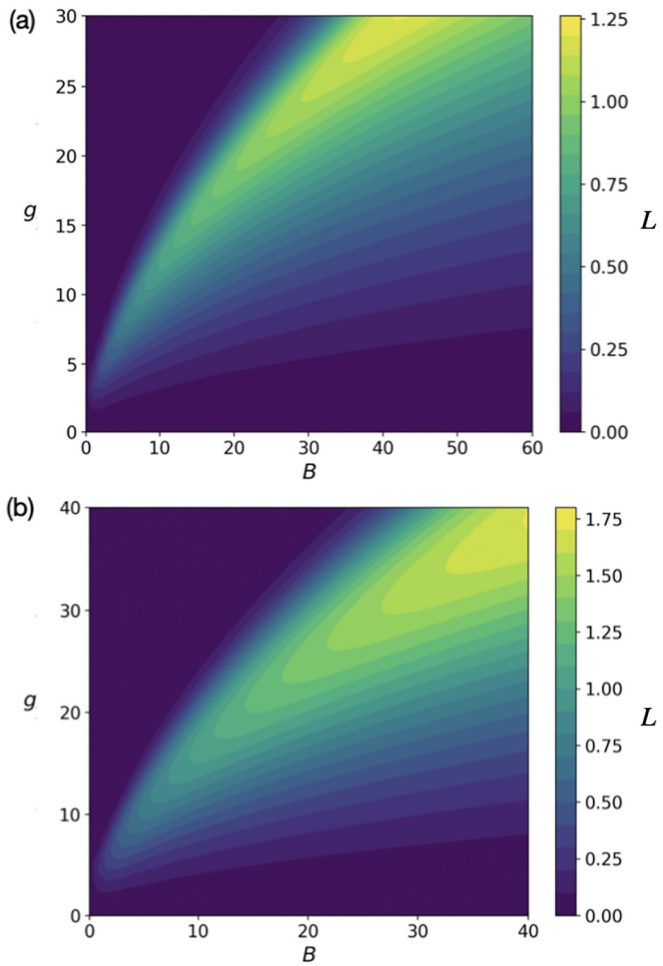

FIG. 9. The numerical calculated angular momentum L for (a) $N = 1$ and (b) $N = 2$ qubits. It is assumed that $\Delta = 1$.

where D_{ph} is the matrix of the bare photon propagator and Π_j is the polarizability matrix of the jth qubit. The photon propagator can be obtained from the equations of motion for the photon canonical coordinate and momentum [30]. In the basis of the x and y polarized modes, the propagator reads

$$D_{ph}(\omega) = \frac{-\omega^2}{(\omega^2-1)^2 - 4B^2\omega^2}\begin{pmatrix} \omega^2-1 & -2i\omega B \\ 2i\omega B & \omega^2-1 \end{pmatrix}, \quad \text{(D2)}$$

where energies are normalized to the bare cavity resonant frequency. We note that the chirality B mixes the linearly polarized components and thus leads to the nondiagonal terms. In the basis of circularly polarized modes, the propagator takes the diagonal form,

$$D_{ph}(\omega) = -\begin{pmatrix} \frac{\omega^2}{(\omega-\omega_r)(\omega+\omega_l)} & 0 \\ 0 & \frac{\omega^2}{(\omega+\omega_r)(\omega-\omega_l)} \end{pmatrix}. \quad \text{(D3)}$$

The qubit polarizability is most readily written in the Cartesian basis. Polarizability Π_j of the jth qubit is a bare bubble with two vertices corresponding to the coupling to the x and y polarized modes. The strength of coupling is proportional to the orientation of dimer $\mathbf{n}_j$. Thus, in the Cartesian basis, the polarizability matrix can be written as

$$\Pi_j(\omega) = -\frac{2\Delta}{\omega^2-\Delta^2}\begin{pmatrix} \cos^2\varphi_j & \cos\varphi_j \sin\varphi_j \\ \cos\varphi_j \sin\varphi_j & \sin^2\varphi_j \end{pmatrix}. \quad \text{(D4)}$$

In the basis of circularly polarized modes, the polarizability matrix reads

$$\Pi_j(\omega) = -\frac{\Delta}{\omega^2-\Delta^2}\begin{pmatrix} 1 & e^{-2i\varphi_j} \\ e^{2i\varphi_j} & 1 \end{pmatrix}. \quad \text{(D5)}$$

The integral in Eq. (D1) can be taken analytically, yielding

$$\delta E_0^{RPA} = \frac{1}{2}\sum_{l=1}^{4}\omega_{pol,l} - \frac{1}{2}(\omega_r+\omega_l) - \Delta, \quad \text{(D6)}$$

where $\omega_{pol,l}$ are the energies of the polaritonic modes in the system which are found as the square roots x_l of the zeros of the following fourth-order polynomial $P(x)$,

$$P(x) = (x-\Delta^2)^2(x-\omega_r^2)(x-\omega_l^2) - \frac{g^2}{2}\Delta x(x-\Delta^2)(x-1) + \frac{g^4}{16}(1-|Z|^2)\Delta^2 x^2, \quad \text{(D7)}$$

where $Z = \frac{1}{N}\sum_{j=1}^{N} e^{i2\varphi_j}$. The roots of the polynomial can be found in the absence of the magnetic field, $\omega_r = \omega_l = 1$, and the result is presented in Eq. (9) in the main text.

[1] F. Schlawin, D. M. Kennes, and M. A. Sentef, Cavity quantum materials, Appl. Phys. Rev. **9**, 011312 (2022).

[2] A. F. Kockum, A. Miranowicz, S. De Liberato, S. Savasta, and F. Nori, Ultrastrong coupling between light and matter, Nat. Rev. Phys. **1**, 19 (2019).

[3] A. Thomas, E. Devaux, K. Nagarajan, T. Chervy, M. Seidel, D. Hagenmüller, S. Schütz, J. Schachenmayer, C. Genet, G. Pupillo *et al.*, Exploring superconductivity under strong coupling with the vacuum electromagnetic field, arXiv:1911.01459.

[4] J. B. Curtis, Z. M. Raines, A. A. Allocca, M. Hafezi, and V. M. Galitski, Cavity quantum Eliashberg enhancement of superconductivity, Phys. Rev. Lett. **122**, 167002 (2019).

[5] M. A. Sentef, M. Ruggenthaler, and A. Rubio, Cavity quantum-electrodynamical polaritonically enhanced electron-phonon coupling and its influence on superconductivity, Sci. Adv. **4**, eaau6969 (2018).

[6] F. Schlawin, A. Cavalleri, and D. Jaksch, Cavity-mediated electron-photon superconductivity, Phys. Rev. Lett. **122**, 133602 (2019).

[7] J. Li and M. Eckstein, Manipulating intertwined orders in solids with quantum light, Phys. Rev. Lett. **125**, 217402 (2020).

[8] Y. Ashida, A. İmamoğlu, J. Faist, D. Jaksch, A. Cavalleri, and E. Demler, Quantum electrodynamic control of matter: Cavity-enhanced ferroelectric phase transition, Phys. Rev. X **10**, 041027 (2020).

[9] D. Guerci, P. Simon, and C. Mora, Superradiant phase transition in electronic systems and emergent topological phases, Phys. Rev. Lett. **125**, 257604 (2020).

[10] X. Wang, E. Ronca, and M. A. Sentef, Cavity quantum electrodynamical Chern insulator: Towards light-induced quantized anomalous Hall effect in graphene, Phys. Rev. B **99**, 235156 (2019).

[11] L. A. Martínez-Martínez, R. F. Ribeiro, J. Campos-González-Angulo, and J. Yuen-Zhou, Can ultrastrong coupling change ground-state chemical reactions? ACS Photon. **5**, 167 (2018).

[12] T. W. Ebbesen, Hybrid light-matter states in a molecular and material science perspective, Acc. Chem. Res. **49**, 2403 (2016).

[13] F. J. Garcia-Vidal, C. Ciuti, and T. W. Ebbesen, Manipulating matter by strong coupling to vacuum fields, Science **373**, eabd0336 (2021).

[14] W. Ahn, J. F. Triana, F. Recabal, F. Herrera, and B. S. Simpkins, Modification of ground-state chemical reactivity via light-matter coherence in infrared cavities, Science **380**, 1165 (2023).

[15] P. Roelli, C. Galland, N. Piro, and T. J. Kippenberg, Molecular cavity optomechanics as a theory of plasmon-enhanced Raman scattering, Nat. Nanotechnol. **11**, 164 (2016).

[16] M. K. Schmidt, R. Esteban, A. González-Tudela, G. Giedke, and J. Aizpurua, Quantum mechanical description of Raman scattering from molecules in plasmonic cavities, ACS Nano **10**, 6291 (2016).

[17] M. Reitz, C. Sommer, B. Gurlek, V. Sandoghdar, D. Martin-Cano, and C. Genes, Molecule-photon interactions in phononic environments, Phys. Rev. Res. **2**, 033270 (2020).

[18] M. Hertzog, B. Munkhbat, D. Baranov, T. Shegai, and K. Börjesson, Enhancing vibrational light-matter coupling strength beyond the molecular concentration limit using plasmonic arrays, Nano Lett. **21**, 1320 (2021).

[19] P. A. Thomas, K. S. Menghrajani, and W. L. Barnes, Cavity-free ultrastrong light-matter coupling, J. Phys. Chem. Lett. **12**, 6914 (2021).

[20] F. Fogliano, B. Besga, A. Reigue, P. Heringlake, L. M. de Lépinay, C. Vaneph, J. Reichel, B. Pigeau, and O. Arcizet, Mapping the cavity optomechanical interaction with subwavelength-sized ultrasensitive nanomechanical force sensors, Phys. Rev. X **11**, 021009 (2021).

[21] S. R. Das, S. Majumder, S. K. Sahu, U. Singhal, T. Bera, and V. Singh, Instabilities near ultrastrong coupling in a microwave optomechanical cavity, Phys. Rev. Lett. **131**, 067001 (2023).

[22] D. E. Chang, J. I. Cirac, and H. J. Kimble, Self-organization of atoms along a nanophotonic waveguide, Phys. Rev. Lett. **110**, 113606 (2013).

[23] M. T. Manzoni, L. Mathey, and D. E. Chang, Designing exotic many-body states of atomic spin and motion in photonic crystals, Nat. Commun. **8**, 14696 (2017).

[24] I. Iorsh, A. Poshakinskiy, and A. Poddubny, Waveguide quantum optomechanics: Parity-time phase transitions in ultrastrong coupling regime, Phys. Rev. Lett. **125**, 183601 (2020).

[25] D. D. Sedov, V. K. Kozin, and I. V. Iorsh, Chiral waveguide optomechanics: First order quantum phase transitions with Z_3 symmetry breaking, Phys. Rev. Lett. **125**, 263606 (2020).

[26] H. B. G. Casimir and D. Polder, The influence of retardation on the London–van der Waals forces, Phys. Rev. **73**, 360 (1948).

[27] B. Munkhbat, A. Canales, B. Küçüköz, D. G. Baranov, and T. O. Shegai, Tunable self-assembled Casimir microcavities and polaritons, Nature (London) **597**, 214 (2021).

[28] D. A. T. Somers, J. L. Garrett, K. J. Palm, and J. N. Munday, Measurement of the Casimir torque, Nature (London) **564**, 386 (2018).

[29] H. Hübener, U. De Giovannini, C. Schäfer, J. Andberger, M. Ruggenthaler, J. Faist, and A. Rubio, Engineering quantum materials with chiral optical cavities, Nat. Mater. **20**, 438 (2021).

[30] D. D. Sedov, V. Shirobokov, I. V. Iorsh, and I. V. Tokatly, Cavity-induced chiral edge currents and spontaneous magnetization in two-dimensional electron systems, Phys. Rev. B **106**, 205114 (2022).

[31] P. Kurilovich, V. D. Kurilovich, J. Lebreuilly, and S. M. Girvin, Stabilizing the Laughlin state of light: Dynamics of hole fractionalization, SciPost Phys. **13**, 107 (2022).

[32] W. Lechner, S. J. M. Habraken, N. Kiesel, M. Aspelmeyer, and P. Zoller, Cavity optomechanics of levitated nanodumbbells: Nonequilibrium phases and self-assembly, Phys. Rev. Lett. **110**, 143604 (2013).

[33] I. V. Tokatly, D. R. Gulevich, and I. Iorsh, Vacuum anomalous Hall effect in gyrotropic cavity, Phys. Rev. B **104**, L081408 (2021).

[34] D. Novokreschenov, A. Kudlis, I. Iorsh, and I. V. Tokatly, Quantum electrodynamical density functional theory for generalized Dicke model, Phys. Rev. B **108**, 235424 (2023).

[35] K. Y. Bliokh and F. Nori, Transverse and longitudinal angular momenta of light, Phys. Rep. **592**, 1 (2015).

[36] G. Giuliani and G. Vignale, *Quantum Theory of the Electron Liquid* (Cambridge University Press, New York, 2008).

[37] F. M. Arscott, *Periodic Differential Equations: An Introduction to Mathieu, Lamé, and Allied Functions* (Elsevier, Amsterdam, 2014), Vol. 66.

[38] J. Dalibard, Collisional dynamics of ultra-cold atomic gases, in *Bose-Einstein Condensation in Atomic Gases* (IOS Press, Netherlands, Amsterdam, 1999), pp. 321–349.

[39] A. Kudlis, D. Novokreschenov, I. Iorsh, and I. V. Tokatly, Nonperturbative effects of deep strong light-matter interaction in a mesoscopic cavity-QED system, Phys. Rev. A **108**, L051701 (2023).

[40] N. Defenu, A. Trombettoni, and S. Ruffo, Criticality and phase diagram of quantum long-range O(N) models, Phys. Rev. B **96**, 104432 (2017).